Investigation of Rechtschaffner and Doehlert approches to elaborate the NiFe2O4 thin film

Nabil Hosni, Wafa Selmi, Karim Zehani, Frédéric Mazaleyrat, Hager Maghraoui-Meherzi

Investigation of experimental design methodology to elaborate $NiFe_2O_4$ thin film by eco-friendly method

N. Hosni[a*], W. Selmi[b], K. Zehani[c], F. Mazaleyrat[d], and H. Maghraoui-Meherzi[a]

[a] *University of Tunis El Manar, Faculty of Science, Laboratory of Analytical Chemistry and Electrochemistry, Campus, 2092 Tunis, Tunisia.*

** Corresponding author: e-mail: nabil.hosni@fst.utm.tn*

[b] *Laboratory of Nanomaterials and Renewable Energy Systems, Research and Technology Center of Energy, Borj-Cedria Science and Technology Park, BP 95, 2050 Hammam-Lif, Tunisia*

[c] *CMTR, ICMPE, UMR 7182, CNRS Paris Est Créteil University, 2-8 rue Henri Dunant, F-94320, Thiais, France.*

[d] *SATIE, ENS Paris-Saclay, CNRS, Universite Paris-Saclay, 4 avenue des sciences, 91190 Gif-sur-Yvette, France.*

Highlights

- Experimental design methodology has been applied to investigate the influence of the principal experimental parameters on saturation magnetization.
- Optimal condition of $NiFe_2O_4$ thin film has been investigated by Doehlert matrix.
- The obtained $NiFe_2O_4$ thin film was elaborated by chemical bath deposition.
- Electrochemical properties of $NiFe_2O_4$ thin film have been investigated in 1M NaOH aqueous electrolyte.

Abstract

The experimental design methodology has been applied to determine the influence of the experimental parameters and their interaction on saturation magnetization (M_s) of thin films. The saturation magnetization (M_s) is very influenced by the deposition and annealing temperature which is proved by Rechtschaffner design. The optimal condition of the $NiFe_2O_4$ thin film has been predict by Doehlert matrix. The prepared $NiFe_2O_4$ thin film under optimal condition synthesized by a green chemistry method, was characterized by XRD, FTIR and Raman spectrometer for structural and phase identification. The flower-like structure of the $NiFe_2O_4$ thin film has been revealed by SEM analysis. The ferrimagnetic behavior of the $NiFe_2O_4$ elaborated at the optimal conditions has been determined by VSM measurement. The measured saturation magnetization (0.49 T) agrees with M_s (0.48 T) predict by Rechtschaffner design. The double-layer capacitance (EDLC) of $NiFe_2O_4$ has been investigated by cyclovoltammetry which show a semi-rectangular shape in the negative and positive potential

and the electrochemical impedance spectroscopy confirm the resistance behavior of the $NiFe_2O_4$ electrode.

Keywords: $NiFe_2O_4$ thin film, Chemical bath deposition (CBD), Rechtschaffner design, Magnetic properties, Electrochemical properties.

1. Introduction

The inverse Spinel ferrites with $Fd\bar{3}m$ space group are a class of materials with general structure of AFe_2O_4 (A corresponds to Mn^{+2}, Fe^{2+}, Co^{2+}, Ni^{2+}, etc…) where the divalent ions switch with half of trivalent ions between tetrahedral and octahedral sites [1]. The ferrites are most prepared in bulk for this many researchers developed ferrites in nanoparticles or thin films [2, 3]. However, thin film materials, plays critical role in the development of ferrite materials with great properties [4] and performance [5]. In fact, the synthesis conditions affect mostly the materials characteristics such as crystallinity, homogeneity, porosity, roughness [6].

The ferrite thin films are attractive due to their remarkable ferromagnetic properties as unique magnetic structure, high saturation magnetization (M_s), high magnetic anisotropy, low magnetic coercivity, and remarkable electrochemical and thermal stability, which render them suitable for many applications, such as electronics devices [7], magnetic information storage [8], microwave absorption [9], photocatalysis [10], supercapacitors [11], lithium ion batteries [12], electrochemical sensor [13], gas sensors [14], fuel cells [15], etc.

Thus, ferrite thin films were successfully synthesis by several techniques which can be categorized into physical and chemical methods. The physical methods which include pulsed laser deposition (PLD) [16], molecular beam epitaxy (MBE) [17] and RF magnetron sputtering [18], however the chemical methods consist electrodeposition [19], sol-gel [20], spin-spraying [21], spin coating [22], dip-coating [23], successive ionic layer adsorption and reaction (SILAR) [24], reflux [25], chemical vapor deposition (CVD) [26] and chemical bath deposition (CBD) [27]. Otherwise, the chemical bath deposition (CBD) has many advantageous, the low-cost, the simply, the rapidity and the ecology of this technique. Also, the CBD method can offer the control of the preparative parameters such as precursor concentration, deposition time, bath temperature, pH, etc. However, the possibility to control thus parameters allowed us to use experimental design methodology.

The experimental design [28] is become very useful to perform the optimization of the variables and preliminary studies of experimental parameters such as the temperature of

deposition (T_d), the time of deposition (t_d), the concentration, the pH, the annealing temperature (T_R) etc. Traditional univariate approaches are performed by varying each experimental parameter independently of the others, while Rechtschaffner designs represents the best solution to perform the optimization of many variables. However, the motivation behind the use of Rechtschaffner and Doehlert designs [29] in the current study is mainly due to its minimal number of experimental runs that does not compromise with the quality of the achieved results and a clear identification between different factor interactions.

In this study, we use the experimental design methodology to investigate the influence of the principal experimental parameters such as temperature deposition (T_d), time deposition (t_d), R' = [Fe]/[OH^-] parameter, pH, annealing temperature (T_R) and annealing time (t_R) on the saturation magnetization (M_s) of $NiFe_2O_4$ thin film. The optimal conditions for the deposition of $NiFe_2O_4$ thin film has been studied using Doehlert matrix. The obtained thin film into the optimal conditions elaborate by chemical bath deposition has been examined by X-ray diffraction technique, Raman , FTIR, scanning electron microscopy, vibrating sample magnetometer, cyclovoltammetry and Electrochemical Impedance Spectroscopy to study the structural, spectroscopic, morphological, magnetic and electrochemical properties respectively.

2. Experimental details

All the chemical precursors used in this work were purchased from Aldrich and used without further purification.

2.1. Preparation of optimal $NiFe_2O_4$ thin film

The optimal $NiFe_2O_4$ thin film has been deposited by low-cost chemical bath deposition (CBD) in stainless steel (SS) substrates. The stainless steel (SS) substrate has been polished by polish paper and cleaned with deionized water to remove unwanted oxides formed on the surface. The cleaned stainless steel (SS) substrate was immersed in the basic solution of iron chloride and nickel chloride under constant stirring for 2 h. Then, the film has been taken out from the bath and washed with de-ionized water to remove the excess of particles and finally, the film has been annealed in oven.

2.2. Characterization of optimal $NiFe_2O_4$ thin film

The NEMROD Software program [30] has been used to determine the optimal condition of the $NiFe_2O_4$ thin film. The structure of the $NiFe_2O_4$ thin film has been confirmed by X-ray diffraction technique at room temperature with a scanning range of $2\theta = 20 - 90^\circ$ using a D8

advanced X-ray diffractometer (λ(Cu-Kα) = 1.5406 Å). Fourier transform infrared (FTIR) and Raman were utilized to identify chemical bonds of $NiFe_2O_4$ thin film in the range of 200-4000 cm^{-1}. The surface morphology of the film has been studied by Merlin scanning electron microscopy (SEM) equipped with Silicon Drift Detector (SDD)-X-Max 50 from Oxford Instrument. The magnetic behaver of the prepared thin film has been recorded by Vibrating Sample Magnetometer (VSM) at room temperature with maximum applied field of ±15 kA/m. The cyclovoltammetry (CV), the electrochemical impedance spectroscopy (EIS) and the tafel polarization have been performed at room temperature using PGZ–402 potentiostat with a three-electrode cell. The CV, the measurements were recorded in a solution of 1 M NaOH in the potential range of -0.5 to 0.5 V at the scan rate of 100 mVs^{-1} and the EIS measurements were carried out in open circuit potential in the frequency range of 1 Hz -100 KHz.

Results and discussion

2.3. Influence of the operating parameters on saturation magnetization (M_s) of $NiFe_2O_4$ thin film using Rechtschaffner design

In order to evaluate the influence of operating parameters on saturation magnetization (M_s) of the $NiFe_2O_4$ thin films six main parameters (factors) were chosen: deposition temperature (U_1), deposition time (U_2), concentration ratio R' = $[Fe]/[OH^-]$ (U_3), pH (U_4), annealing temperature (U_5) and annealing time (U_6). To determine the influence of these six factors and their interaction on saturation magnetization (M_s) of thin films a two-level full factorial design 2^{k-p} was used. In these types of designs, variables (*k*) are set at two levels (minimum) and (maximum) normalized as (-1) and (+1). The linear polynomial model of the experimental response associated to (2^{6-1}) factorial design (for 6 variables) was represented by the following equation:

$$Y = b_0 + b_1X_1 + b_2X_2 + b_3X_3 + b_4X_4 + b_5X_5 + b_6X_6 + b_{12}X_1X_2 + b_{13}X_1X_3 + b_{23}X_2X_3 + b_{14}X_1X_4 + b_{24}X_2X_4 + b_{34}X_3X_4 + b_{15}X_1X_5 + b_{25}X_2X_5 + b_{35}X_3X_5 + b_{45}X_4X_5 + b_{16}X_1X_6 + b_{26}X_2X_6 + b_{36}X_3X_6 + b_{46}X_4X_6 + b_{56}X_5X_6 \quad (1)$$

Were:

Y: experimental response (saturation magnetization (M_s))

X_i: coded variable (-1 or +1)

b_i: estimation of the principal effect of the factor i for the response Y

b_{ij}: estimation of interaction effect between factor i and j for the response Y.

Table 1. Experimental domain investigated for $NiFe_2O_4$ thin films

Coded variables (X_i)	Factors (U_i)	Unit	Experimental field	
			Lower limit	Upper limit
X_1	U_1: deposition temperature (T_d)	°C	40	70
X_2	U_2: deposition time (t_d)	min	60	180
X_3	U_3: R' = [Fe]/[OH^-]	-	1.11	1.75
X_4	U_4: pH	-	9	10
X_5	U_5: annealing temperature (T_R)	°C	550	750
X_6	U_6: annealing time (t_R)	h	4.30	6

The variables for the model was chosen referring to previous work [31]. The coefficients of the equation model were calculated in the experimental field are listed in **Table 1** and the results are represented in the **Table 2**. The coefficients of the linear polynomial model are calculated using only extremes by NEMROD Software program [30] which is represented in the following equation:

$$Y = 141.665 + 19.072\ X_1 + 2.643\ X_2 - 8.514\ X_3 - 6.508\ X_4 + 29.910\ X_5 - 4.980\ X_6 - 0.845\ X_1X_2 - 5.155\ X_1X_3 + 7.022\ X_2X_3 - 9.656\ X_1X_4 - 4.097\ X_2X_4 - 0.934\ X_3X_4 + 12.426\ X_1X_5 + 3.482\ X_2X_5 - 4.410\ X_3X_5 - 7.203\ X_4X_5 - 1.549\ X_1X_6 - 3.442\ X_2X_6 - 3.610\ X_3X_6 - 7.673\ X_4X_6 + 5.183\ X_5X_6 \quad (2)$$

Table 2. Experimental domain investigated for $NiFe_2O_4$ thin films

Experimental number	Experimental design						Experimental plan						Results Y (T)
	X_1	X_2	X_3	X_4	X_5	X_6	U_1	U_2	U_3	U_4	U_5	U_6	
1	-1	-1	-1	-1	-1	-1	40	60	1.11	9	550	4.30	0.112
2	-1	1	1	1	1	1	40	180	1.75	10	750	6	0.156
3	1	-1	1	1	1	1	70	60	1.75	10	750	6	0.18
4	1	1	-1	1	1	1	70	180	1.11	10	750	6	0.231
5	1	1	1	-1	1	1	70	180	1.75	9	750	6	0.282
6	1	1	1	1	-1	1	70	180	1.75	10	550	6	0.093
7	1	1	1	1	1	-1	70	180	1.75	10	750	4.30	0.232
8	1	1	-1	-1	-1	-1	70	180	1.11	9	550	4.30	0.169
9	1	-1	1	-1	-1	-1	70	60	1.75	9	550	4.30	0.143
10	1	-1	-1	1	-1	-1	70	60	1.11	10	550	4.30	0.181
11	1	-1	-1	-1	1	-1	70	60	1.11	9	750	4.30	0.286
12	1	-1	-1	-1	-1	1	70	60	1.11	9	550	6	0.180
13	-1	1	1	-1	-1	-1	40	180	1.75	9	550	4.30	0.145
14	-1	1	-1	1	-1	-1	40	180	1.11	10	550	4.30	0.151
15	-1	1	-1	-1	1	-1	40	180	1.11	9	750	4.30	0.182
16	-1	1	-1	-1	-1	1	40	180	1.11	9	550	6	0.111
17	-1	-1	1	1	-1	-1	40	60	1.75	10	550	4.30	0.162
18	-1	-1	1	-1	1	-1	40	60	1.75	9	750	4.30	0.138
19	-1	-1	1	-1	-1	1	40	60	1.75	9	550	6	0.106
20	-1	-1	-1	1	1	-1	40	60	1.11	10	750	4.30	0.185
21	-1	-1	-1	1	-1	1	40	60	1.11	10	550	6	0.112
22	-1	-1	-1	-1	1	1	40	60	1.11	9	750	6	0.156

As can be seen in **Fig.1a** the saturation magnetization is very influenced by the annealing temperature (b_5 = 0.038) as it has a positive response on the studied. In fact. the increasing of annealing temperature leads to increase the saturation magnetization. The second most significant factor is the temperature of deposition (b_1 = 0.024) which have positive effect on the studied response. There is a significant X_1X_5 interaction between the deposition and the annealing temperature (b_{15} = 0.016). Thus, the effect of the deposition temperature (X_1) depends on the annealing temperature (X_5) in the chosen range and vice versa which has a positive effect on the response. Note also that the effects of the other factors are very negligible.

The Pareto analysis gave more significant information to interpret the results of Rechtschaffner design. In fact, the advantage of this analysis is the calculation of the percentage effect of each factor on the response. The numerical values of this analysis are given by the following relation:

$$P_i = \left(\frac{b_i^2}{\sum b_i^2}\right) \times 100 \qquad (3)$$

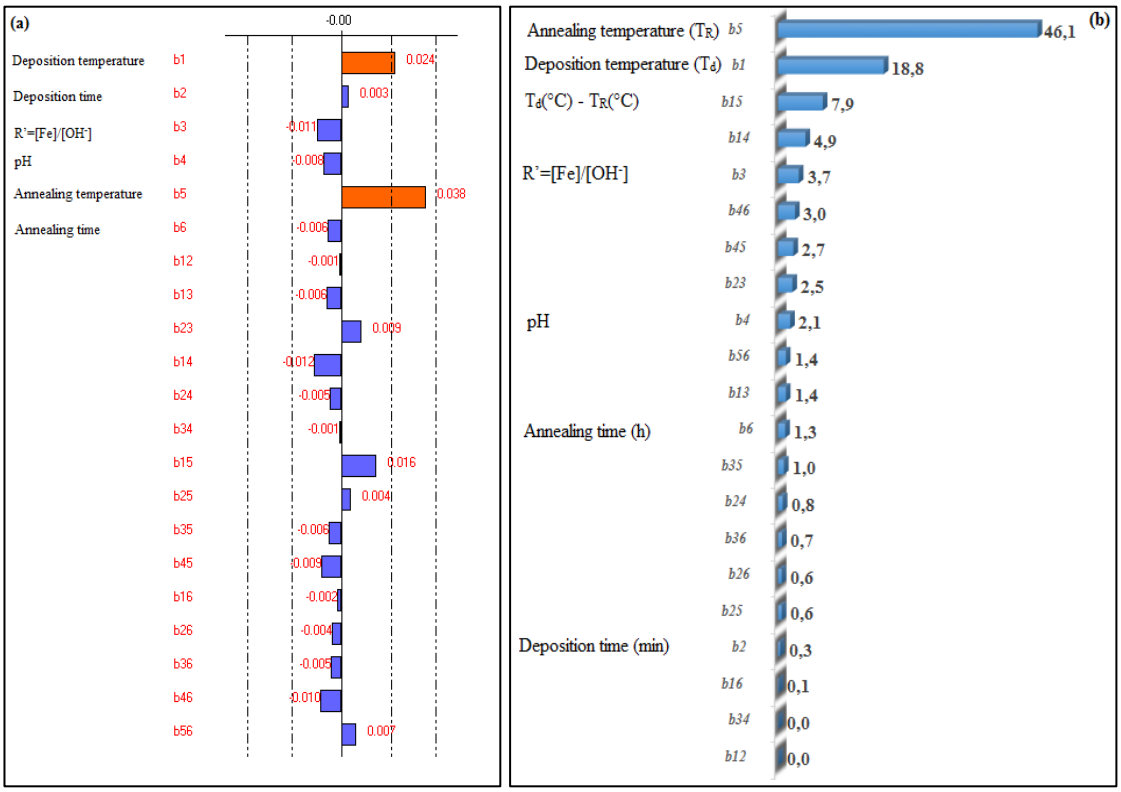

Fig. 1. (a) Graphical analysis of the effect of : deposition temperature, deposition time, R′, pH, annealing temperature and time, (b) Graphical Pareto analysis.

As can be seen in Pareto graphic analysis (**Fig.1b**), the annealing temperature is the most influential factors on the saturation magnetization with 46.1% contribution response. And the second parameters which influence on the saturation magnetization is the temperature of

deposition with total contribution of 18.7%. Furthermore, those factors have an important and meaningful positive interaction with a contribution of 64.8%. We can note also, that more than 72.7% of the response are bringing by the two factors and their interaction. However, the pH, R′, deposition and annealing time and their interactions have a negligible effect with only 27.3% of the response.

2.4. Determination of the optimal condition of $NiFe_2O_4$ thin film using Doehlert design

In order to determine the optimal condition of $NiFe_2O_4$ thin film, the approach of Doehlert was applied after determination of the most influential parameters on saturation magnetization. The annealing and deposition temperature are the two factors determined in Rechtschaffner approach which will be investigated in the Doehlert study. The advantages of this approach are the ability to explore the whole of the experimental domain through a minimum number of experiments and the possibility to extend the domain by adding another factor.

Table 3. Experimental domain investigated for $NiFe_2O_4$ thin films

Coded variables (X_i)	Factors (U_i)	Unit	Experimental domain	
			Lower limit	Upper limit
X_1	U_1: annealing temperature	°C	550	750
X_2	U_2: deposition temperature	°C	40	70

The Doehlert approach is formed by uniformly distributed of the experimental points within the space filling of the coded variables (X_i). To compare the effects of those factors U_i cited previously in the experimental domain (**Table.3**), concerned coded variables were used. For calculation, the experimental value of the factors U_1 and U_2 were transformed into coded X_1 and X_2 using the following relation:

$$X_i = \frac{U_i - \bar{U}_i}{\Delta U_i} \quad (4)$$

where: X_i is the value taken by the coded variable i, Ui is the value taken by the factor i, $\bar{U}_i$ is the value taken by the factor i in the center of the experimental field and ΔUi is the range of variation of the factor i.

$$\overline{U_I} = \frac{(upper\ limit\ of(U_i) + lower\ limit\ of\ (U_i))}{2} \quad (5)$$

$$\Delta U_i = \frac{(upper\ limit\ of(U_i) + lower\ limit\ of\ (U_i))}{2\gamma_i} \quad (6)$$

The experimental response (saturation magnetization (M_s)) associated to the Doehlert approach can be described as following by a second-degree quadratic polynomial equation:

$$Y = b_0 + b_1X_1 + b_2X_2 + b_{11}X_1^2 + b_{22}X_2^2 + b_{12}X_1X_2 \quad (7)$$

Where:

Y: the experimental response (saturation magnetization (M_s));

b_0: an independent term; bi: the coefficients of the linear terms;

b_{ii}: the coefficients of the quadratic terms;

b_{ij}: the coefficients corresponding to the interaction term between the factor i and the factor j.

In addition, the calculation of the coefficients of this model was carried through the least squares method:

$$B = (X^T X)^{-1} \times X^T \times Y \quad (8)$$

where:

B: is the estimates coefficients vector;

X^T: is the transposed model matrix;

X: is the model matrix;

Y: is the measured response vector.

Using Doehlert approach, the number of experiments (N) required is given by the following relation: $N = k + k^2 + 1$, where k is the number of factors. As mentioned previously two factors influence on the saturation magnetization consequently, 7 different experiments were required. However, in order to validate this model, three replicated experiments at the center level were carried out. Doehlert matrix, experimental plan and results for the two selected factors were listed in **Table.4**.

Table 4. Experimental domain investigated for $NiFe_2O_4$ thin films

Experimental number	**Experimental design**		**Experimental plan**		**Results Y(T)**
	X_1	X_2	U_1	U_2	
1	1.0000	0.0000	750	55	0.427
2	-1.0000	0.0000	550	55	0.115
3	0.5000	0.8660	700	70	0.277
4	-0.5000	-0.8660	600	40	0.154
5	0.5000	-0.8660	700	40	0.453
6	-0.5000	0.8660	600	70	0.142
7	0.0000	0.0000	650	55	0.366
8	0.0000	0.0000	650	55	0.365
9	0.0000	0.0000	650	55	0.366

Based to these results, the coefficients of the polynomial model were calculated using NEMROD Software program mentioned above:

$$Y = 291{,}58 + 140{,}432\ X_1 - 42{,}456\ X_2 - 75{,}73\ X_1^2 - 87{,}49\ X_2^2 - 73{,}933\ X_1X_2 \quad (9)$$

The effects of the various factors: annealing temperature and deposition temperature were quantified respectively by b_1 and b_2 as well as their interactions b_{12}. **Figure.2** represents the effects of the various factors as well as their interactions. The annealing temperature has a positive effect (b_1 = 140.43) on M_s of the material, so any increase in the annealing temperature increases the value of M_s. The deposition temperature has a negative effect (b_2 = -42.45) on the value of M_s. It can be noted that the annealing temperature is the most influential factor on the response of M_s.

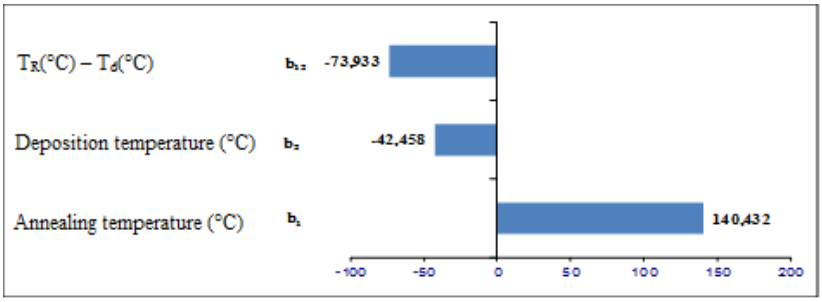

Fig. 2. Graphical analysis of the effect of deposition temperature and annealing temperature.

To confirm this result, we plotted the response surface curves in 3D as well as the isoresponse curves. **Figure.3** shows the isoreponse curve of M_s as a function of annealing temperature and deposition temperature and the 3D surface of M_s in the plane (T_R, T_d).

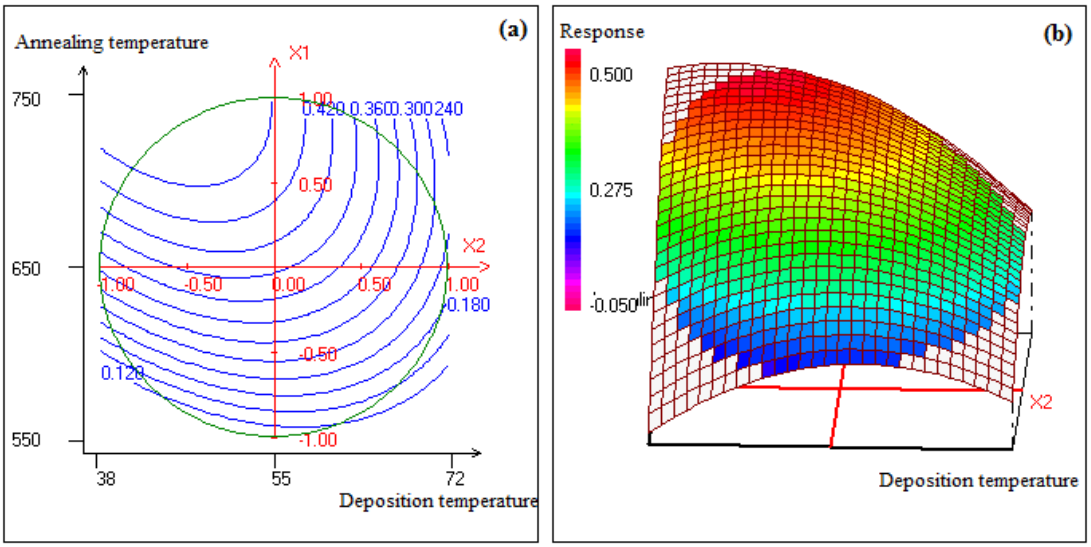

Fig. 3. (a) Contour plots of saturation magnetization (M_s) versus deposition temperature (°C) and annealing temperature (°C), (b) The corresponding three-dimensional plot.

The effects of interaction between deposition and annealing temperature on saturation magnetization were represented in **Fig.3**. As can be seen, the maximums of the saturation magnetization (M_s) of $NiFe_2O_4$ are obtained for annealing temperatures tend around 750 °C. In addition, to improve the response studied, it would be useful to increase the annealing temperature for deposition temperatures below 60 °C. Consequently, the optimal working condition that allows the formation of $NiFe_2O_4$ thin film with a maximum M_s (0.48 T) was found at: T_R = 739 °C and T_d = 47 °C.

2.5. Characterization of the optimal condition of $NiFe_2O_4$ thin film

The structural properties of $NiFe_2O_4$ thin film prepared under optimal conditions determined from Doehlert matrix, is investigated by X-ray diffraction. **Figure. 4a** shown the X-ray diffractogramme of $NiFe_2O_4$ thin film. The observed reflection peaks located at 30.13°, 35.50°, 44.47°, 57.19°, 74.93° were assigned to the (2 2 0), (3 1 1), (4 0 0), (5 1 1) and (5 3 3) planes respectively which correspond to the spinel ferrite $NiFe_2O_4$ with a cubic symmetry, and Fd-3m space group. Whereas, peaks located at 43.59°, 50.86° and 74.68° were attributed to stainless steel (SS) substrate. The obtained pattern found to be in good agreement with the JCPDS files (Card No.10-325) which confirmed the formation of cubic $NiFe_2O_4$ phase.

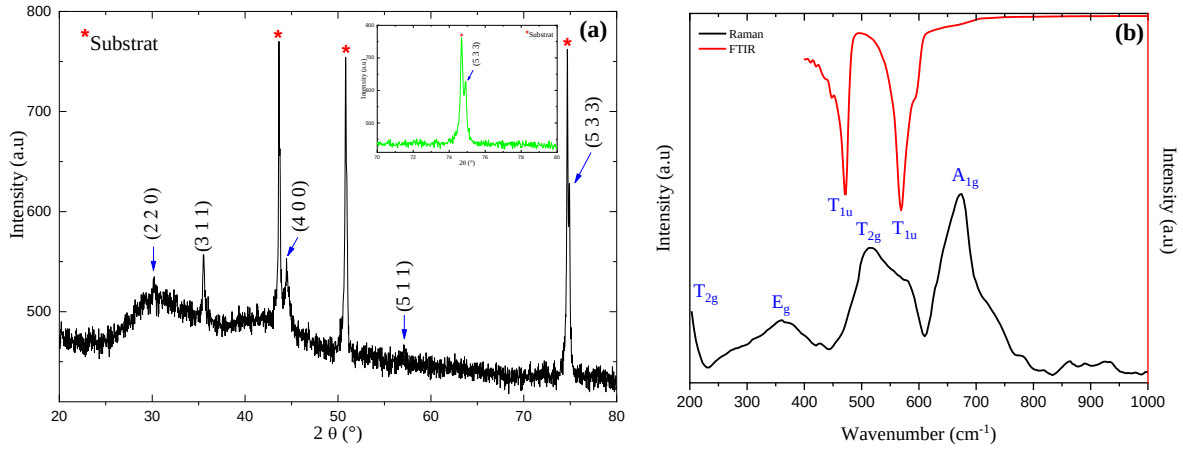

Fig. 4. (a) X-ray diffraction pattern and (b) Raman, FTIR spectra of $NiFe_2O_4$ thin film deposited at T_R = 739 °C and T_d = 47 °C.

The average crystallite size (D), microstrain (ε) and dislocation density (δ) of the optimal condition of $NiFe_2O_4$ thin film were determined using the following relations:

$$D = \frac{k\lambda}{\beta \cos\theta} \tag{10}$$

$$\varepsilon = \frac{\beta}{4 \tan\theta} \tag{11}$$

$$\delta = \frac{1}{D^2} \quad (12)$$

Where:

k is the Scherrer constant, λ is the Cu(Kα) radiation wavelength, β is the full width at half-maximum (FWHM) and θ is the diffraction Bragg angle.

The crystallite size (D), microstrain (ε) and dislocation density (δ) determined from the above formulas were found to be in the order of 38 nm, 0.40 and 6.92 10^{14} m^{-2} respectively. It is well known that the magnetic parameters for the complex oxides strongly depend on the average and distribution of crystallite size.

Raman and FTIR spectra of the thin film is presented in **Fig. 4b**. All these peaks and bands can be attributed to $NiFe_2O_4$. The peaks at 202 and 516 cm^{-1} are assigned to T_{2g} modes, and those at 359 and 673 cm^{-1} are assigned to E_g and A_{1g} modes respectively. The bands located at 470 and 568 cm^{-1} in FTIR spectra are assigned to Nickel ferrite ($NiFe_2O_4$) sample. The band at 359 cm^{-1} exhibits the stretching vibrations due to Ni-O and the band at 568 cm^{-1} correspond to stretching vibrations of Fe-O. The spectroscopy analysis confirms the formation of spinel structure of $NiFe_2O_4$ found in structural study.

The energy dispersive X-ray spectrometry (EDX) was used to determine the elemental composition of the obtained film. The EDX spectra shows (**Fig.5**) that the Fe/Ni atomic percentage was detected by a ratio of $R_{Fe/Ni}$ =2 which confirms the formation of stoichiometric ferrite nickel thin film with absence of any impurity. As can be seen, the Ni, Fe and O signals are higher than the C signal. This large amount of C into the film is derived from the double-sided carbon tape of SEM measurements confirmed by element mapping images. SEM images (**Fig.5**) demonstrate that the elaborated film has a good coverage with flower-like structure, which is formed by the assembly of flower petal layers. The average crystallite sizes deduced from image treatments for the film are in the range of 52 and 118 nm. However, the homogeneous distribution of Ni, Fe and O was observed also in the element mapping images.

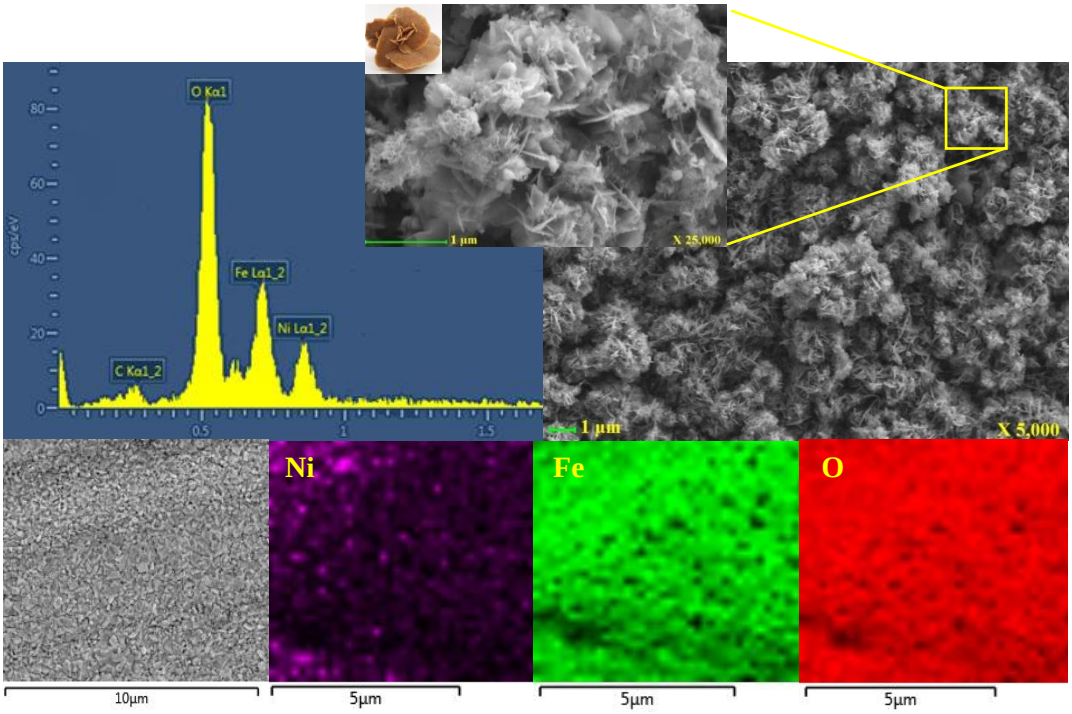

Fig. 5. EDX spectra, SEM image with corresponding elemental mapping images of $NiFe_2O_4$ thin film deposited at T_R = 739 °C and T_d = 47 °C.

In order to correlate the result found in Doehlert methodology to magnetic properties, hysteresis loops (M–H curve) for $NiFe_2O_4$ thin film prepared under optimal conditions was investigated. The Magnetic hysteresis loops measured in and out-of-plane in the field range of ±15 kA/m at room temperature are shown in **Fig.6**.

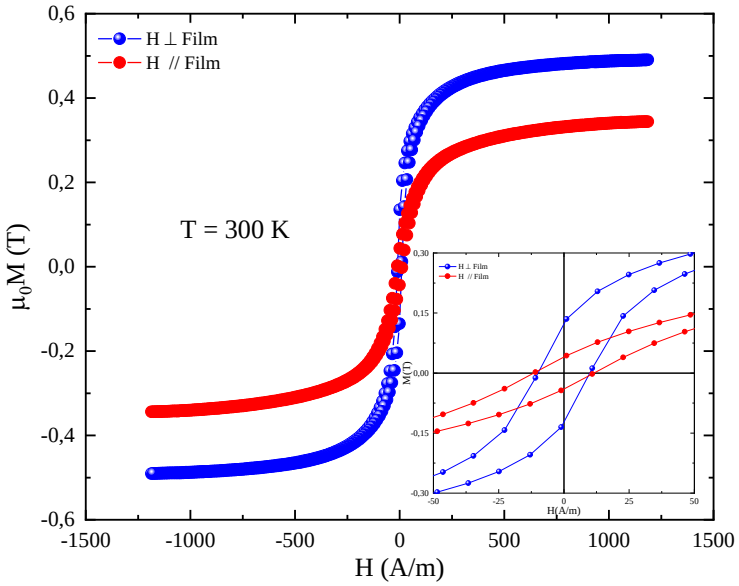

Fig. 6. M-H hysteresis loops of $NiFe_2O_4$ thin film deposited at T_R = 739 °C and T_d = 47 °C.

The in-plane measurement of the $NiFe_2O_4$ thin film has shown a saturation magnetization (M_s) equal to 0.49 T with a coercivity (H_c) of 12.02 kA/m. The magnetocrystalline anisotropy energy [32] was calculated by the following equation:

$$K_u = \frac{H_c M_s}{2}$$

The value of the magnetocrystalline anisotropy energy is equal to 2.95 J/m^3. The sample was rotated perpendicular from the initial position and the hysteresis loop resulting from the out-plane measurement was recorded. The M_s and H_c values significantly increased to 0.34 T and 12.04 kA/m, respectively. However, this significant difference between in-plane and out-of-plane saturation magnetization is due is due to effect of magnetic anisotropy. The $NiFe_2O_4$ thin film exhibits a soft ferrimagnetic behavior at room temperature with a large saturation magnetization.

The electrochemical properties of the $NiFe_2O_4$ were evaluated by CV, EIS, and Tafel polarization measurements within a three-electrode cell in 1 M NaOH aqueous electrolyte.

The CV curves measured at a scan rate of 100 mVs^{-1} are represented in **Fig.7a**. Apparently, the CV curve shows a semi-rectangular shape in the potential window of -0.5 to 0.5 V without any oxidation/reduction peak. The semi-rectangular shape observed in CV curves in the negative and positive potential, indicate the double-layer capacitance (EDLC) of $NiFe_2O_4$ electrode.

To confirm the double layer capacitance of the $NiFe_2O_4$ electrode the EIS measurement has been study. The Nyquist plot and the equivalent circuit are shown in **Fig.7b**. Nyquist plot consist two parts, a semicircle in the high-frequency region and a straight line in the low-frequency region. The large radius of the semicircle is assigned to the charge transfer resistance of the electrode and the vertical line is attributed to the dominant capacitive behavior of the electric double layer formed at the electrode/ electrolyte interface. The values of R_s, R_{ct}, C and W were estimated qualitatively from the fittings of experimental impedance spectra which are equal to 29.4 Ω, 43.5 Ω, 0.43μF and 0.27 $\Omega.s^{-5}$ respectively.

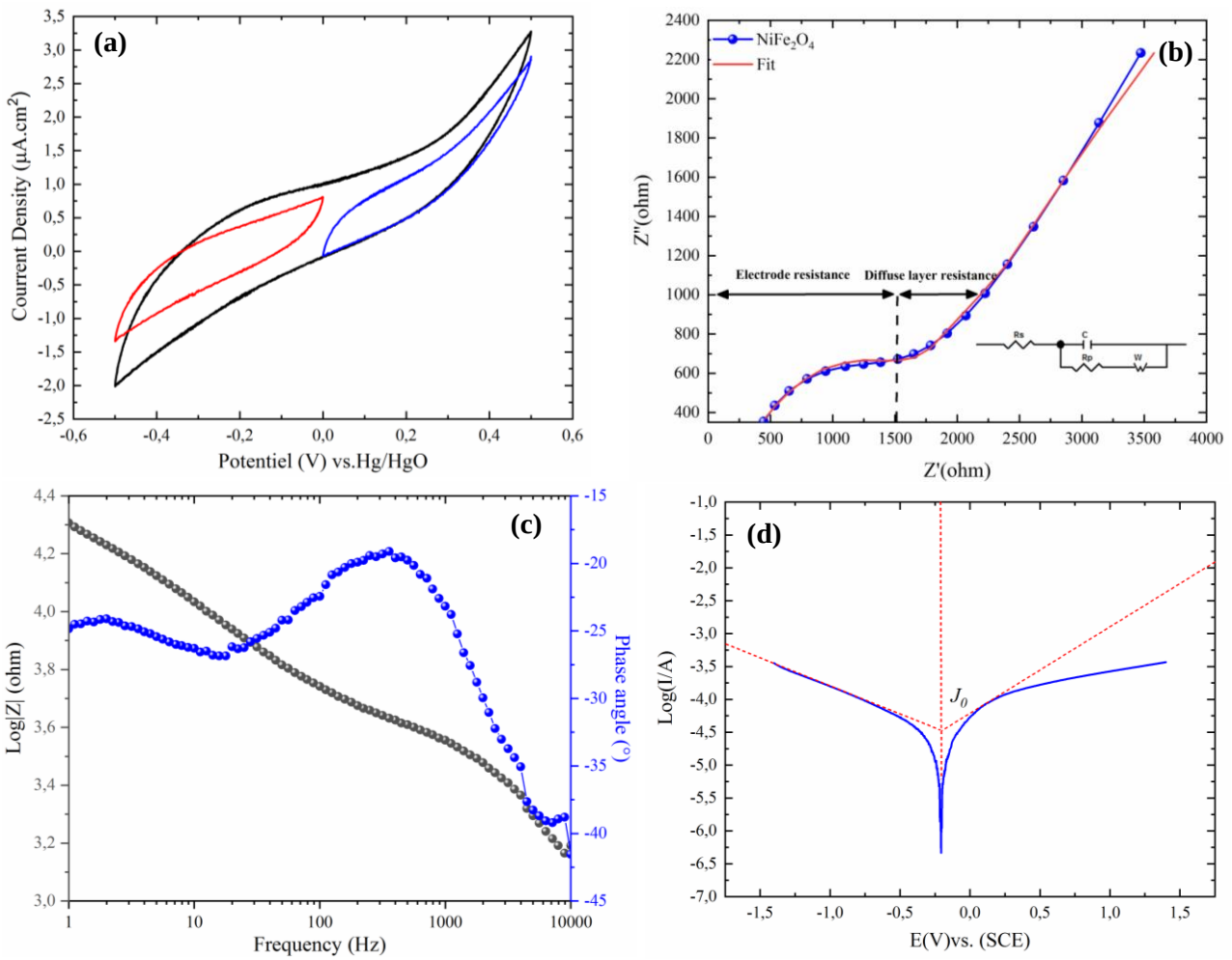

Fig.7. (a) The cyclic voltammograms, (b) Nyquist plot with equivalent circuit, (c) Bode plots and (d) Tafel plot of $NiFe_2O_4$ thin film deposited at T_R = 739 °C and T_d = 47 °C.

The Bode plots (Frequency (Hz) vs. Phase angle (°) and Log |Z|) of the $NiFe_2O_4$ nanoflowers are presented in **Fig.6c**. At low frequency when the phase angle approaches to 90° that indicates the ideal capacitive behavior of the electrode, and when the phase angle is close to 0° that indicates the pure resistance behavior of the material. The phase angle of the prepared $NiFe_2O_4$ thin film, is equal to 19° at low frequency which corresponds to resistance contribution of the electrode. The results of Bode plots confirm the resistance behavior of electrode found in EIS measurement.

The potentiodynamic polarization test was performed just a few minutes after Impedance measurements to determine the corrosion rates of the electrode. The Tafel polarization curve of $NiFe_2O_4$ electrode is shown in **Fig.7d**. The calculation of corrosion potential (E_{corr}) and corrosion current density (I_{corr}) based on the Tafel slope method are equal to -0.2 V and -14.07 µA, respectively.

Conclusion

Rechtschaffner design has been adopted to determine the most influential parameters on saturation magnetization (M_s). In fact, Rechtschaffner design demonstrated that the deposition and annealing temperature are the most influential parameters on M_s. To elaborate the $NiFe_2O_4$ thin film, the optimal condition has been predicted by Doehlert matrix. The spinel structure of the obtained film has been investigated by DRX, Raman and FTIR. The nanoflower morphology of the $NiFe_2O_4$ film has been confirmed by SEM. To correlate the result found in Doehlert methodology to magnetic properties, hysteresis loops (M–H curve) for $NiFe_2O_4$ thin film prepared under optimal conditions has been examined. Electrochemical properties of the $NiFe_2O_4$ film has been tested with three electrodes system in 1 M NaOH electrolyte at room temperature. We believe that the elaborate film can be an excellent electrode for EDLC devices.

Acknowledgements

This work is mainly supported by Ministry of Higher Education and Scientific Research Tunisia and the French National Center for Scientific Research (CNRS).

References

[1] V. Polshettiwar, R. Luque, A. Fihri, H. Zhu, M. Bouhrara, J.M. Basset, Magnetically Recoverable Nanocatalysts, Chem. Rev. 111 (2011) 3036-3075. https://doi.org/10.1021/cr100230z.

[2] N. Hosni, K. Zehani, T. Bartoli, L. Bessais, and H. Maghraoui-Meherzi, Semi-hard magnetic properties of nanoparticles of cobalt ferrite synthesized by the co-precipitation process, J. Alloys Compd. 694 (2017) 1295-1301. https://doi.org/10.1016/j.jallcom.2016.09.252.

[3] C. Solís, S. Somacescu, E. Palafox, M. Balaguer, J. M. Serra, Particular transport properties of $NiFe_2O_4$ thin films at high temperatures, J. Phys. Chem. C 118 (2014) 24266–24273. https://doi.org/10.1021/jp506938k.

[4] L. Kumar, P. Kumar, M. Kar, Effect of non-magnetic substitution on the structural and magnetic properties of spinel cobalt ferrite ceramics, J. Mater. Sci: Mater. electron. 24 (2013) 2706-2715. https://doi.org/10.1021/acs.chemmater.5b01034.

[5] A. Hao, M. Ismail, S. He, N. Qin, R. Chen, A. M. Rana, D. Bao, Enhanced resistive switching and magnetic properties of Gd-doped $NiFe_2O_4$ thin films prepared by chemical solution deposition method, Mater. Sci. Eng., B. 229 (2018) 86-95. https://doi.org/10.1016/j.mseb.2017.12.025.

[6] S. B. Bandgar, M. M. Vadiyar, Y. C. Ling, J. Y. Chang, S. H. Han, A. V. Ghule, S. S. Kolekar, Metal Precursor Dependent Synthesis of $NiFe_2O_4$ Thin Films for High-Performance Flexible Symmetric Supercapacitor, ACS Appl. Energy Mater. 1 (2018) 638–648. https://doi.org/10.1021/acsaem.7b00163.

[7] J. Li, H. Huang, P. Qiu, Z. Liao, X. Zeng, Y. Lu, C. Huang, Topotactic fluorination induced stable structure and tunable electronic transport in perovskite barium ferrite thin films, Ceram. 46 (2020) 8761-8765. https://doi.org/10.1016/j.ceramint.2019.12.115.

[8] L. Kumar, P. Kumar, M. Kar, Effect of non-magnetic substitution on the structural and magnetic properties of spinel cobalt ferrite ceramics, J. Mater. Sci: Mater. electron. 24 (2013) 2706-2715. https://doi.org/10.1021/acs.chemmater.5b01034.

[9] M. M. Ismail, S. N. Rafeeq, J. M. A. Sulaiman, A. Mandal, Electromagnetic interference shielding and microwave absorption properties of cobalt ferrite $CoFe_2O_4$/polyaniline composite, Appl. Phys. A. 124 (2018) 380-392. https://doi.org/10.1007/s00339-018-1808-x.

[10] A. Kalam, A. G. Al Sehemi, M. Assiria, G. Du, T. Ahmadd, I. Ahmad, M. Pannipar, Modified solvothermal synthesis of cobalt ferrite ($CoFe_2O_4$) magnetic nanoparticles photocatalysts for degradation of methylene blue with H_2O_2/visible light, Results Phys. 8 (2018) 1046-1053. https://doi.org/10.1016/j.rinp.2018.01.045.

[11] A. Soam, R. Kumar, C. Mahender, M. Singh, D. Thatoi, Rajiv O. Dusane, Development of paper-based flexible supercapacitor: Bismuth ferrite/graphene nanocomposite as an active electrode material, J. Alloys. Compd. 15 (2020) 152145-152155. https://doi.org/10.1016/j.jallcom.2019.152145.

[12] T. D. Dongale, S. S. Khot, A. A. Patil, S. V. Wagh, P. B. Patil, D. P. Dubal, T. G. Kim, Bifunctional nanoparticulated nickel ferrite thin films: Resistive memory and aqueous battery applications, Mater. Des. 201 (2021) 109493-109504. https://doi.org/10.1016/j.matdes.2021.109493.

[13] A. S. Ganie, S. Bano, S. Sultana, S. Sabir, M. Z. Khan, Ferrite Nanocomposite Based Electrochemical Sensor: Characterization, Voltammetric and Amperometric Studies for Electrocatalytic Detection of Formaldehyde in Aqueous Media, Electroanalysis. 33 (2021) 233-248. https://doi.org/10.1002/elan.202060179.

[14] P. Rao, R.V.Godbole, S. Bhagwat, Nanocrystalline Pd:$NiFe_2O_4$ thin films: A selective ethanol gas sensor, J. Magn. Magn. Mater. 416 (2016) 292-298. https://doi.org/10.1016/j.jmmm.2016.05.021.

[15] M. Rethinasabapathy, A.T. E. Vilianb, S. K. Hwang, S. M. Kang, Y. Cho, Y. K. Han, J. K. Rhee, Y. S. Huh, Cobalt ferrite microspheres as a biocompatible anode for higher power generation in

microbial fuel cells, J. Power Sources. 483 (2021) 229170. https://doi.org/10.1016/j.jpowsour.2020.229170.

[16] Md. Kashif Shamim, S. Sharma, R. J. Choudhary, Lead-free (K, Na, Li) NbO_3/$NiFe_2O_4$ thin films by pulsed laser deposition: Structure, dielectric, magnetic and magnetodielectric behavior, J. Alloys Compd. 794 (2019) 534-541. https://doi.org/10.1016/j.jallcom.2019.04.201.

[17] W. Huang, J. Zhu, H. Z. Zeng, X. H. Wei, Y. Zhang, Y. R. Li, Strain induced magnetic anisotropy in highly epitaxial $CoFe_2O_4$ thin films, Appl. Phys. Lett. 89 (2006) 262506. https://doi.org/10.1063/1.2424444.

[18] J. Shan, A. V. Singh, L. Liang, L. J. Cornelissen, Z. Galazka, A. Gupta, B. J. van Wees, T. Kuschel, Enhanced magnon spin transport in NiFe2O4 thin films on a lattice-matched substrate, Appl. Phys. Lett. 113, 162403 (2018). https://doi.org/10.1063/1.5049749.

[19] S. D. Sartale, C. D. Lokhande, M. Giersig, V. Ganesan, Novel electrochemical process for the deposition of nanocrystalline $NiFe_2O_4$ thin films, J. Phys.: Condens. Matter. 16 (2004) 773-783. https://doi.org/10.1088/0953-8984/16/6/008.

[20] S. Seifikar, T. Rawdanowicz, W. Straka, C. Quintero, N. B. Gharbbc, J. Schwartz, Structural and magnetic properties of sol–gel derived $NiFe_2O_4$ thin films on silicon substrates, J. Magn. Magn. Mater. 361 (2014) 255-261. https://doi.org/10.1016/j.jmmm.2014.03.004.

[21] M. Ran, Z. Yu, K. Sun, C. Wu, H. Qing, H. Liu, Z. Lan, X. Jiang, Effects of aqueous ethanol solutions on the structural and magnetic properties of NiZn ferrite thin films prepared by spin-spray deposition, Cermic. 2021. https://doi.org/10.1016/j.ceramint.2021.02.119.

[22] S. Ben Khalifa, M. Gassoumi, A. Ben Dhahbi, F. Alresheedi, A. Z. elAbdeen, Mahmoud, L. Beji, The effect of the cobalt ferrites nanoparticles ($CoFe_2O_4$) on the porous silicon deposited by spin coating, Alex. Eng. J. 59 (2020) 1093-1098. https://doi.org/10.1016/j.aej.2019.12.031.

[23] P. Byung-Geon, Bismuth ferrite thin film coated on polycarbonate surface and its photocatalytic properties in visible light, Mater. Lett. 285 (2021) 129006. https://doi.org/10.1016/j.matlet.2020.129006.

[24] V. Kumar, H. S. Panda, Observation of morphology resembling Hydrangea macrophylla flower in SILAR-deposited MFe_2O_4 ($M=Co^{2+}$, Ni^{2+}, Mn^{2+}) nanocrystallites: synergetic effect on electrochemical performance, Nanotechnology. 31 (2020) 415402. https://doi.org/10.1088/1361-6528/ab9e29.

[25] A. Manohar, V. Vijayakanth, R. Hong, Solvothermal reflux synthesis of $NiFe_2O_4$ nanocrystals dielectric and magnetic hyperthermia properties, J. Mater. Sci.: Mater. Electron. 31 (2020) 799-806. https://doi.org/10.1007/s10854-019-02588-z.

[26] R. Datta, B. Loukya, N. Li, A. Gupt, Structural features of epitaxial $NiFe_2O_4$ thin films grown on different substrates by direct liquid injection chemical vapor deposition, J. Crystal Growth. 345 (2012) 44-50. https://doi.org/10.1016/j.jcrysgro.2012.02.007.

[27] J. L. Gunjakar, A. M. More, V. R. Shinde, C. D. Lokhande, Synthesis of nanocrystalline nickel ferrite ($NiFe_2O_4$) thin films using low temperature modified chemical method, J. Alloys Compd. 465, (2008) 468-473. https://doi.org/10.1016/j.jallcom.2007.10.130.

[28] A. Kesraoui Abdessalem, N. Oturan, N. Bellakhal, M. Dachraoui, M. A. Oturan, Experimental design methodology applied to electro-Fenton treatment for degradation of herbicide chlortoluron, Appl. Catal. B Environ. 78 (2008) 334-341. https://doi.org/10.1016/j.apcatb.2007.09.032.

[29] A. Hannachi, S. Hammami, N. Raouafi, H. Maghraoui-Meherzi, Preparation of manganese sulfide (MnS) thin films by chemical bath deposition: Application of the experimental design methodology, J. Alloys Compd. 663 (2016) 507-515. https://doi.org/10.1016/j.jallcom.2015.11.058.

[30] Mathieu, D., Luu, R. P. T., 1980. Software NEMROD, Université d'Aix-Marseille III, France.

[31] N. Hosni, N. Bouaniza, W. Selmi, K. Assili, H. Maghraoui-Meherzi, Synthesis and physico-chemical investigations of $AgSbS_2$ thin films using Doehlert design and under DFT framework, J. Alloys Compd. 778 (2018) 913-923. https://doi.org/10.1016/j.jallcom.2018.11.072.

[32] J. Singh, S. K. Gupta, A. K. Singh, P. Kothari, R. K. Kotnala, J. Akhtar, Investigation of structural and magnetic properties of Ni, NiFe and $NiFe_2O_4$ thin films, Journal of Magnetism and Magnetic Materials 324 (2012) 999-1005. https://doi.org/10.1016/j.jmmm.2011.10.009.